Properties of Metal-Supported Oxide Honeycomb Monolayers: M 2 O 3 and MM'O 3 on Me(111) (M, M' = Ti, V, Cr, Fe; Me = Ag, Au, Pt)

Jacek Goniakowski, C. Noguera

Properties of Metal-Supported Oxide Honeycomb Monolayers: M_2O_3 and $MM'O_3$ on Me(111) (M, M′=Ti, V, Cr, Fe; Me=Ag, Au, Pt)

J. Goniakowski* and C. Noguera*

CNRS-Sorbonne Université, UMR 7588, INSP, F-75005 Paris, France

E-mail: jacek.goniakowski@insp.jussieu.fr; claudine.noguera@insp.jussieu.fr

Abstract

With the help of a DFT+U approach, we have analyzed the characteristics of a series of pure and mixed $3d$ transition metal oxide honeycomb monolayers of M_2O_3 and MM'O_3 stoichiometries (M, M' = Ti, V, Cr and Fe) deposited on a metal substrate (Me = Ag, Au, Pt). We show that the substrate-induced structural polarization, interfacial electron transfer, and oxide-metal interaction strength display general trends which are governed by the offsets between the oxide band structure and the metal Fermi level. They are the strongest for the least electronegative cations (Ti and V) deposited on supports with the largest work functions (Au, Pt), where the depletion of purely $3d$ Ti and V states provokes an increase of the cation oxidation state. Mixing generally induces electron transfers from the least (Ti and V) to the most (Cr and Fe) electronegative cations. However, the systematic delocalization of the Ti_2O_3 d valence electrons to the metal substrates limits any significant mixing-induced electronic rearrangements to the V-based compounds only. We show that these electronic effects directly impact the energetics of cationic mixing and are responsible for a dramatic destabilization of the mixed $TiFeO_3$ monolayers compared to the bulk ilmenite phase, while they stabilize ordered mixed $VFeO_3$ films which have no bulk equivalent. Our findings give general guidelines on how oxide electronic, magnetic and reactivity characteristics can be efficiently engineered by tuning the oxide stoichiometry and the metal substrate, of direct interest for modern technologies.

1 Introduction

Aside from van der Waals two-dimensional (2D) materials such as graphene, silicene, germanene, hexagonal boron nitride, or transition metal dichalcogenides, oxide monolayers (MLs) have recently attracted more and more interest due to their promising applications in the fields of catalysis and corrosion protection and to their relevance in the process of high-temperature oxide encapsulation of noble metal catalysts. Their properties are strongly affected by their reduced size and low dimensionality, which allows a large flexibility of their stoichiometry, atomic structure and electronic characteristics, often leading to complex compounds which have no bulk equivalents.[1,2] Moreover, the growing demand of methods for engineering the properties of such two-dimensional objects, fosters an efficient use of cation doping or mixing. Indeed, combining cations of different size, electronegativity and reducibility, may give a lever for modifying the oxide structural, electronic, and chemical reactivity characteristics.

Among the most frequently encountered oxide monolayer structures, the M_2O_3 honeycomb (HC) one, which consists of a fully-coordinated network of twelve member rings with an equal number of oxygen and metal atoms, has been extensively studied experimentally and theoretically, whether freestanding,[3] or Pd(111)-,[4,5] Pt(111)-,[6,7] Au(111)-supported[5,8–12] as well as sandwiched between Al_2O_3 films.[13] Aside its occurrence in sesquoxides monolayers, oxide honeycomb films have also been observed in Cu_3O_2/Au(111),[14] or used as a template for a synthesis of supported ternary $Ba_xTi_2O_3$/Au(111) compounds.[15]

Regarding cationic doping and mixing, we have recently shown that the low dimensionality of freestanding M_2O_3 HC MLs and their peculiar, flat atomic structure determine their specific electronic characteristics (gap width, character of gap edges) and are responsible for cation redox reactions and mixing preferences which are different from those in the corresponding three-dimensional mixed oxides.[3] However, if these results provide guidelines for understanding properties of oxide films supported on very weakly interacting substrates, they are likely less relevant for the case of metal supports, which are the most widely used in practical realizations. Indeed, in another recent study, we have shown that the atomic structure of Au-supported M_2O_3 HC MLs is characterized by a large structural rumpling and that the electronic characteristics of the freestanding films are severely altered by a charge exchange with the gold substrate, which in extreme cases may result in a change of cation oxidation state.[9]

In this context, the goal of the present theoretical work is twofold. On the one hand, beyond Au-supported M_2O_3 MLs considered in our previous work,[9] we analyze the substrate-induced characteristics of pure M_2O_3 and mixed MM'O_3 oxide films (M, M' = Ti, V, Cr, and Fe) deposited on three metallic substrates (Me = Ag, Au and Pt) of higher and higher work functions. Relying on DFT+U results on freestanding and Me-supported MLs, we identify the mechanisms responsible for the most essential structural, electronic, and energetic characteristics of these supported films. On the other hand, at variance with mixing at weakly or non interacting interfaces,[3] we consider realistic situations by explicitly including the interaction with a metal substrate. To this goal we link the electronic and energetic characteristics of mixed MM'O_3/Me compounds to those of their pure M_2O_3/Me and M'$_2O_3$/Me parents and we assess the roles played by the character of the latter (Mott-Hubbard or charge transfer) and by the substrate work function.

The paper is organized as follows. After a section devoted to the computational method and set-up (Sec. 2), we report the results on Me-supported pure M_2O_3 MLs (Sec. 3) and mixed MM'O_3 MLs (Sec. 4). These results are then discussed in Sec. 5, before a conclusion.

2 Computational details

DFT calculations were performed with the Vienna Ab-initio Simulation Package (VASP)[16,17] using the Projector Augmented Wave (PAW) method[18,19] to represent the electron-core interaction and a 400 eV energy cut-off in the development of Kohn-Sham orbitals on a plane-wave basis set. We have checked that an increase of the cut-off to 500 eV does not bring any noticeable modifications to the reported results. For example, for $VFeO_3$ and its parents Fe_2O_3 and V_2O_3, regardless of the underlying metal, it changes the structural characteristics (film rumpling, anion-cation and cation-substrate bond lengths) by less than 0.01 Å, the electronic characteristics (anion, cation, and substrate charges) by less than 0.01 e/f.u. and the energetic ones (mixing energy) by less than 0.01 eV/f.u.

Dispersion-corrected (optB88-vdW)[20–22] exchange-correlation functional was employed, within the DFT+U approach proposed by Dudarev.[23,24] As in our previous studies,[3,9,25,26] we have used U values close to those reported in the literature: $U = 1$ eV for Ti_2O_3, $U = 1.7$ eV for V_2O_3, $U = 3$ eV for Cr_2O_3 and Fe_2O_3. Moreover we have performed complementary calculations using the HSE03 hybrid approach[27,28] to test the sensitivity of our results to the choice of the exchange-correlation

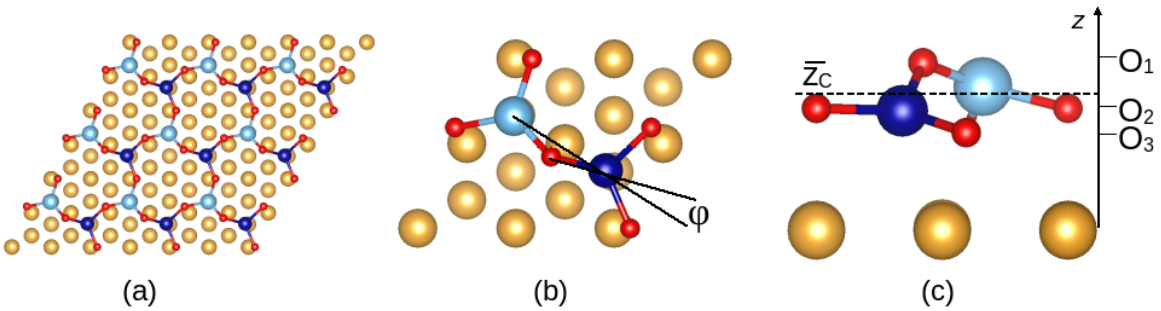

Figure 1: Atomic structures of Me-supported MM'O_3 oxide ML: (a) top view; (b) enlarged top view showing the rotation ϕ of the MO_3 entities; c: enlarged profile view showing the rumpling of the layer, with the two cations and the three oxygen atoms at different elevations. The dashed line represents the average cation elevation $\overline{z_c}$. Cations, oxygen and substrate atoms are represented by blue (dark and light), red, and golden balls, respectively.

functional (Supporting Information (SI), Sections S2). As discussed in details in the case of FeO_x/Pt,[29] and pointed out in studies on CuO_2/Au[14,30] and MgO/Ag,[31] despite the known difficulties of the Hartree-Fock approach to describe metals, the hybrid approximation to the DFT gives a satisfactory description of a metal/oxide interface and thus enables to account for the oxide-metal band offset.

All calculations were spin-polarized and the relative stability of simple non-magnetic (NM) and magnetic solutions (with either parallel (FM) or anti-parallel (AF) spin moments) was systematically tested. Ionic charges were estimated with the partition scheme proposed by Bader[32,33] and magnetic moments were obtained by integration of the spin density within the Bader's volumes. Atomic configurations were plotted with VESTA.[34]

We have considered Me(111)-supported pure M_2O_3 (the parents) and mixed MM'O_3 monolayers (M, M' = Ti, V, Cr, and Fe; Me = Ag, Au and Pt) in an honeycomb structure, Figure 1. All of them were modelled in a (2×2)-Me(111) unit cell, with a single M_2O_3 or MM'O_3 formula unit per cell, at the Me experimental bulk lattice parameter (2.89 Å, 2.88 Å, and 2.765 Å for Ag, Au and Pt, respectively), consistently with experimental observations of pseudomorphic growth of ML Ti_2O_3 on Au(111)[10] and V_2O_3 on Pd(111).[4] The sampling of the Brillouin zone was performed with the Γ-centered (14×14×1) Monkhorst-Pack mesh.[35] The metal substrates were represented by slabs composed of four (111) atomic layers. Increasing the metal thickness up to 6 atomic layers yields negligible corrections on all quantities, consistently with marginal (less than 0.05 eV) changes of the metal work functions. The oxide film was deposited on one side of the metal slab. Beyond the symmetric film structures assumed in Ref.,[9] all atomic coordinates of anions and cations have been allowed to fully relax until forces got lower than 0.01 eVÅ^{-1}. Atoms in the metal substrates were relaxed only in the direction normal to the surface. In the following, the atomic structure of supported MLs will be systematically quantified by the average film rumpling R (defined as a difference of average vertical positions of anions and cations $\overline{z_O} - \overline{z_C}$) and by the average rotation of MO_3 entities $\phi = \angle(M' - M - O)$ projected on the surface plane, Fig. 1.

Adhesion energies between the oxide monolayers and the metal substrates $E_{adh}(Me)$ were calculated from energy differences between the constituted oxide/metal system $E^{oxide/Me}$ and its separated components (bare metal substrate E^{Me} and freestanding oxide ML at its equilibrium lattice parameter E^{oxide}):

$$E_{adh}(Me) = E^{Me} + E^{oxide} - E^{oxide/Me} \quad (1)$$

With this definition, adhesion energies are positive if adhesion is favored.

Formation or mixing energies E_{mix} of both

freestanding and supported MM'O_3 monolayers were calculated from energy differences between the mixed oxide $E^{MM'O_3}$ and the average of the two corresponding parents $(E^{M_2O_3} + E^{M'_2O_3})/2$:

$$E^{MM'O_3}_{mix} = E^{MM'O_3} - \frac{E^{M_2O_3} + E^{M'_2O_3}}{2} \quad (2)$$

With this definition, mixing energies are negative if mixing is favored.

Table 1: Main Characteristics of Freestanding and Me-supported (Me = Ag, Au and Pt) M_2O_3 MLs (M = Ti, V, Cr, and Fe): Film Rumpling R (Å), In-Plane Rotation ϕ (°), Bader Charges on Cations Q_M (e) and Oxygen Atoms Q_O (e), Total Charge of Metal Substrate Q_{Me} (e/M_2O_3 f.u.), and Cation Magnetic Moments μ_M (μ_B).

	Ti_2O_3	V_2O_3	Cr_2O_3	Fe_2O_3
freestanding				
Q_M	1.78	1.69	1.62	1.64
Q_O	-1.19	-1.13	-1.08	-1.10
μ_M	0.9	2.1	3.1	3.9
Ag-supported				
R	0.60	0.41	0.09	0.09
ϕ	14	17	10	19
Q_M	1.92	1.72	1.55	1.44
Q_O	-1.06	-1.04	-1.08	-1.07
μ_M	0.0	1.4/1.5	3.0	3.8
Q_{Ag}	-0.67	-0.33	+0.15	+0.33
Au-supported				
R	0.68	0.68	0.54	0.23
ϕ	10	1	14	20
Q_M	2.00	1.83	1.65	1.53
Q_O	-1.02	-0.96	-0.96	-1.01
μ_M	0.0	1.2	2.7	3.8
Q_{Au}	-0.94	-0.77	-0.42	-0.02
Pt-supported				
R	0.70	0.75	0.47	0.29
ϕ	19	11	17	24
Q_M	2.00	1.87	1.65	1.50
Q_O	-1.01	-0.92	-0.96	-0.98
μ_M	0.0	0.5	2.5	3.8
Q_{Pt}	-0.98	-0.98	-0.44	-0.06

3 Results on supported M_2O_3 monolayers

We first present the computational results for the M_2O_3 HC monolayers (M = Ti, V, Cr, and Fe) supported on the three Me(111) substrates (Me = Ag, Au and Pt). Table 1 and Figure 2 report their main structural, electronic, and magnetic characteristics.. The comprehensive set of results, is given in SI, Tabs. S1 and S2. HSE03 results for the M_2O_3/Au system (M = Ti, V, Cr, and Fe) are given in Tab. S7 and Fig. S1. In the following, the notation Δ will refer to differences between quantities (positions, distances, charges, etc) in the supported and freestanding films

Fully relaxed freestanding oxide MLs systematically adopt a symmetric nearly planar geometry ($R \sim 0$ and $\phi \sim 0$). The only exception is the freestanding Cr_2O_3 monolayer, for which we find a non-vanishing rumpling ($R = 0.06$ Å). The interaction with the metal substrates and the in-plane compression associated to the lattice mismatch between the oxide films and metal surfaces ($a_{M_2O_3} > a_{Me}$, SI, Tab. S1) induce film distortion, which consists of in-plane rotations ϕ of the MO_3 entities and of rumpling R. We will show in the discussion that the positive sign of R (the average outward displacement of the oxygen atoms with respect to the cations), its decrease from Ti to Fe (for each substrate), and its increase from Ag to Pt (for each oxide) are principally driven by the behavior of the interface charge transfer Q_{Me}. Beyond the effect of film rumpling, the in-plane rotations ϕ of the MO_3 entities allow a further reduction of the in-plane oxide lattice parameters such that, despite substantial lattice mismatch, the cation-oxygen distances d_{M-O} remain in all cases close to the corresponding values in the freestanding MLs ($|\Delta d_{M-O}/d_{M-O}| < 2\%$, Tab. S1).

From an electronic point of view, the interaction of the oxide layers with the metallic substrates is characterized by an electron exchange between them, leading in most cases to a negative charging of the Me substrates (negative total substrate charge per M_2O_3 unit, Q_{Me}).

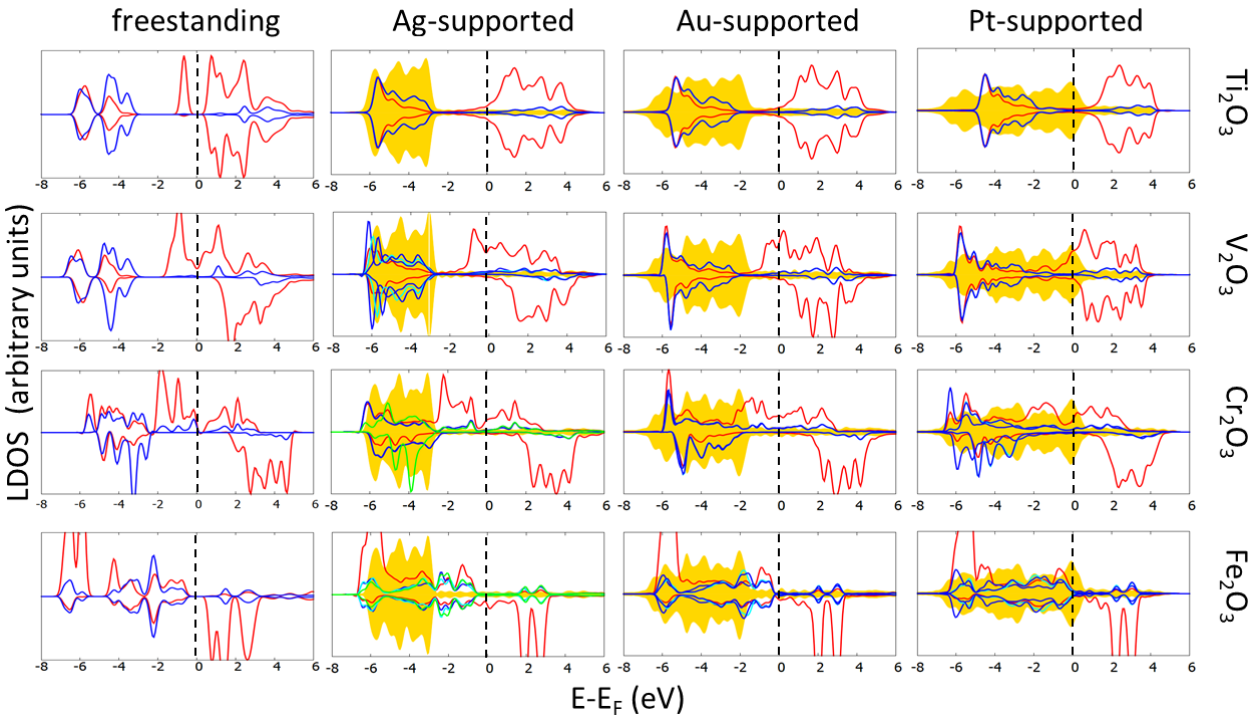

Figure 2: Local densities of states of freestanding and metal-supported M_2O_3 HC MLs (M = Ti, V, Cr, and Fe) projected on cations (red), oxygen atoms (blue), and substrates (golden shading). A broadening of 0.2 eV has been systematically applied. The vertical dashed lines indicate the positions of the Fermi levels.

Small positive Q_{Me} are found only for Cr_2O_3 and Fe_2O_3 MLs deposited on the Ag substrate. In the case of Ag and Au surfaces, where the Fermi level is positioned relatively high in the valence *sp* band, the substrate *d* states contribute only little to the interfacial hybridization and the electrons transferred from the oxide film mainly populate the substrate *s* and *p* orbitals. Conversely, since the Fermi level of the Pt substrate falls in its 4*d* band, the Pt *d* states hybridize strongly with those of the oxide film and become populated by the interfacial charge transfer. Finally the Ag electrons transferred towards the Cr_2O_3 and Fe_2O_3 films populate principally the cation *d* states at the bottom of the oxide conduction band. As expected, $|Q_{Me}|$ tends to decrease monotonically from Ti to Fe (for each substrate), following the increase of cation electronegativity, and increases from Ag to Pt (for each oxide), following the increase of the substrate surface work functions (calculated values are 4.8 eV, 5.6 eV, and 6.1 eV for Ag, Au, and Pt, respectively). The negative Q_{Me} result from a cooperative effect of charge modifications on the oxide cations and oxygen atoms, Q_M increasing (except Q_{Fe}) and $|Q_O|$ decreasing when in contact with a support. The relative contributions of the oxygen atoms to $|Q_{Me}|$ increase from Ti to Fe. Positive Q_{Me} are principally associated with a reduction of cation charges, the effect being particularly strong in the Fe_2O_3/Ag case.

Associated to this interfacial electron transfer, the oxide local densities of states (LDOS) are substantially modified. As seen in Figure 2, whatever the substrate, the modifications are particularly strong at the beginning of the series, in the Mott-Hubbard oxides Ti_2O_3 and V_2O_3, where filled Ti and V 3*d* states close to the Fermi level get totally or partially depleted. At variance, due to the mixed oxygen-cation character of their states at the band gap edges, the band structures of Cr_2O_3 and Fe_2O_3 are much less impacted by the interaction with the metallic substrates.[9] For each oxide, the increase of the metal work function from Ag to Pt shifts the substrate Fermi level progressively downwards on the energy scale. As a conse-

quence, in Ti_2O_3 which has a nearly pure Mott-Hubbard character, the Fermi level E_F moves from the bottom of the Ti-like conduction band (CB) on Ag towards the oxide mid-gap on Pt. The single valence d electron characteristic of the freestanding Ti_2O_3 ML is in all cases delocalized towards the underlying metal, which is consistent with the substantial increase of Q_{Ti} and the systematic quenching of μ_{Ti}, Tab. 1. These major modifications of the Ti_2O_3 electronic structure suggest that a change of oxidation state takes place upon deposition. On general grounds, at variance with the unquestionable 3+ cation valence in freestanding MLs, changes of oxidation states in systems with delocalized electrons cannot be assessed merely from Bader charges. It is the concomitant modifications of the LDOS and magnetic moments μ_{Ti} which can be tentatively rationalized by a Ti 4+ oxidation state on the three substrates.

Similarly, in the case of the Mott-Hubbard oxide V_2O_3, the progressive downward shift of the Fermi level within the majority vanadium band explains the increase of Q_V and the decrease of μ_V along the Ag, Au, Pt series. These results are consistent with a progressive increase of the vanadium oxidation state in V_2O_3 monolayer supported on the three metal substrates. However, changes of V-O hybridization induced by film distortions and the hybridization between cation and substrate states (particularly strong in case of Pt) impede a robust and fully reliable assignment of oxidation states in the three cases.

Finally, in Cr_2O_3 and Fe_2O_3 the shape of the oxide LDOS in the vicinity of the Fermi level is very similar on the three substrates. Consistently, changes of Q_M and μ_M with respect to the freestanding references are similarly small on the three substrates and suggest that the cation 3+ oxidation states are essentially not altered.

To summarize, the interaction with the metal substrates induces structural distortions of the oxide MLs and an electron transfer from the oxides towards the metal, which both increase from Ag to Pt and decrease from Ti to Fe. Only when Cr_2O_3 and Fe_2O_3 are deposited on Ag a small amount of electrons is transferred from the substrate towards the oxide film. The substrate-induced change of oxide electronic and magnetic characteristics is particularly pronounced in Ti_2O_3 and V_2O_3, where it can be associated to an increase of cation oxidation state. If the single Ti valence electron tends to be systematically transferred to the metal substrate, the cation charge of supported V_2O_3 increases progressively from Ag to Pt. Conversely, the much weaker electronic modifications found for Cr_2O_3 and Fe_2O_3 suggest the preservation of the cation 3+ oxidation state characteristic of the freestanding MLs. These conclusions are well supported by the HSE03 results (SI, Tab. S7).

4 Results on supported MM'O_3 monolayers

DFT+U results for the main structural, electronic and magnetic characteristics of freestanding and Me-supported mixed MM'O_3 HC MLs (M, M' = Ti, V, Cr, and Fe; Me = Ag, Au, Pt) are given in Table 2 and Figures 3 and 4. The complete set of results can be found in SI, Tabs. S4 and S5, in which the symbols δ denote the mixing-induced differences between quantities (positions, distances, charges, etc) in the supported mixed oxides and their parents. HSE03 results for mixed MLs on the Au substrate are reported in SI, Tab. S8 and Fig. S2.

From a structural point of view, the metal-supported mixed oxide films are qualitatively similar to their supported parents. They systematically display a substantial (positive) rumpling and in-plane rotations of MO_3 entities which enable an accommodation of the interface lattice mismatch without strong modifications of the cation-oxygen distances d_{M-O} and $d_{M'-O}$ ($|\Delta d_{M-O}/d_{M-O}| < 4\%$, Tab. S4). Contrary to the parent systems, in the mixed films the two cations are systematically not coplanar. Cationic mixing produces a quite substantial rumpling enhancement ($\delta R \sim 0.15$ - 0.25 Å) in $VCrO_3$/Ag, $VFeO_3$/Pt, and $CrFeO_3$/Pt, but in $TiFeO_3$/Ag, $TiCrO_3$/Au, and $VCrO_3$/Au, R is reduced ($\delta R \sim$ -0.10 Å), Tab. S4. We will show in the discussion that the positive sign and the

Table 2: Main Characteristics of Metal (Ag, Au, and Pt)-Supported Mixed MM'O_3 HC Monolayers (M, M' = Ti, V, Cr, and Fe): Film Rumpling R (Å), In-Plane Rotation ϕ (°), Bader Charges on Cations Q_M, Q'_M (e) and Oxygen Atoms Q_O (e), Metal Substrate Charge Q_{Me} (e/MM'O_3 f.u.), and Cation Magnetic Moments μ_M, $\mu_{M'}$ (μ_B).

	$TiVO_3$	$TiCrO_3$	$TiFeO_3$	$VCrO_3$	$VFeO_3$	$CrFeO_3$
freestanding						
Q_M, $Q_{M'}$	1.75,1.69	1.80,1.55	2.09, 1.33	1.84, 1.47	1.87, 1.35	1.67, 1.60
Q_O	-1.15	-1.12	-1.14	-1.10	-1.08	-1.09
μ_M, $\mu_{M'}$	1.0, 2.0	0.9, 3.2	0.1, 3.6	1.4, 3.6	1.3, 3.6	2.7, 4.0
Ag-supported						
R	0.50	0.41	0.23	0.47	0.35	0.06
ϕ	15	19	19	18	19	18
Q_M, $Q_{M'}$	1.91,1.73	1.93,1.58	1.95,1.38	1.81,1.46	1.82,1.35	1.60,1.37
Q_O	-1.05	-1.06	-1.09	-1.00	-1.01	-1.08
μ_M, $\mu_{M'}$	0.2,1.4	0.2,2.9	0.1,3.7	0.7,3.4	0.,3.7	2.6,3.7
Q_{Ag}	-0.47	-0.33	-0.05	-0.27	-0.15	0.27
Au-supported						
R	0.69	0.52	0.45	0.49	0.50	0.35
ϕ	5	16	19	16	16	20
Q_M, $Q_{M'}$	1.99,1.86	2.01,1.67	2.01,1.54	1.93,1.51	1.94,1.42	1.69,1.51
Q_O	-0.99	-1.02	-1.03	-0.98	-0.96	-1.00
μ_M, $\mu_{M'}$	0.1,0.9	0.1,2.8	0.1,3.9	0.5,3.4	0.0,3.7	2.2,3.9
Q_{Au}	-0.88	-0.60	-0.45	-0.50	-0.48	-0.21
Pt-supported						
R	0.74	0.61	0.52	0.68	0.67	0.62
ϕ	15	20	24	18	18	19
Q_M, $Q_{M'}$	1.97,1.91	1.98,1.69	2.00,1.55	1.94,1.62	1.96,1.49	1.75,1.47
Q_O	-0.95	-0.97	-1.00	-0.92	-0.91	-0.89
μ_M, $\mu_{M'}$	0.0,0.0	0.1,2.3	0.1,4.0	0.3,2.8	0.1,3.9	1.3,3.9
Q_{Pt}	-1.04	-0.76	-0.54	-0.80	-0.70	-0.55

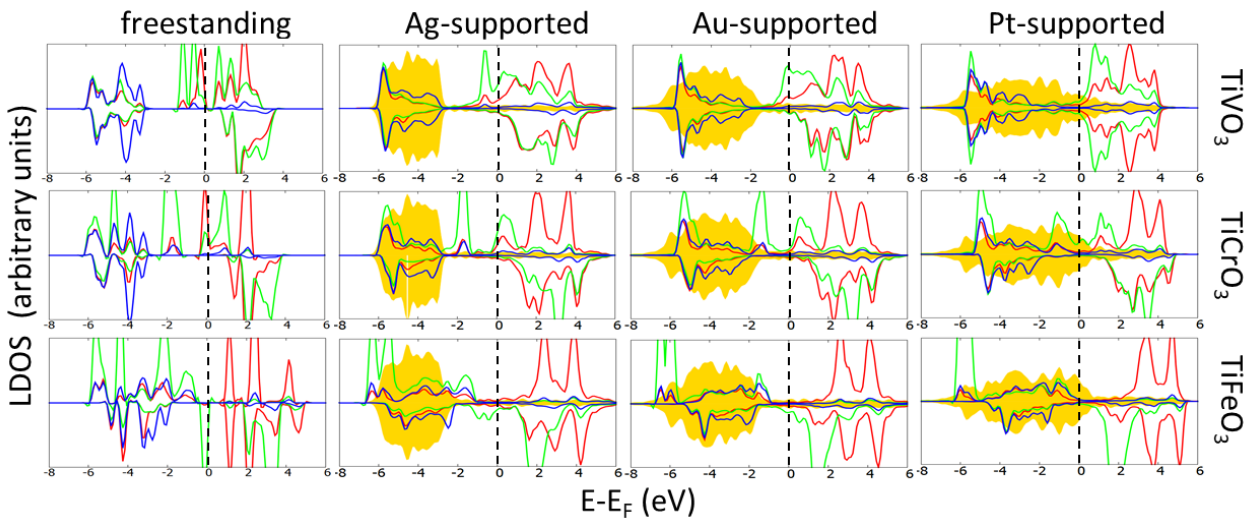

Figure 3: Local densities of states in freestanding and Me-supported mixed TiM'O_3 honeycomb monolayers (M' = V, Cr, Fe) projected on Ti (red), M' (green), O atoms (blue), and substrate atoms (gold shading). A broadening of 0.2 eV has been systematically applied. Vertical dashed lines indicate the position of the Fermi level.

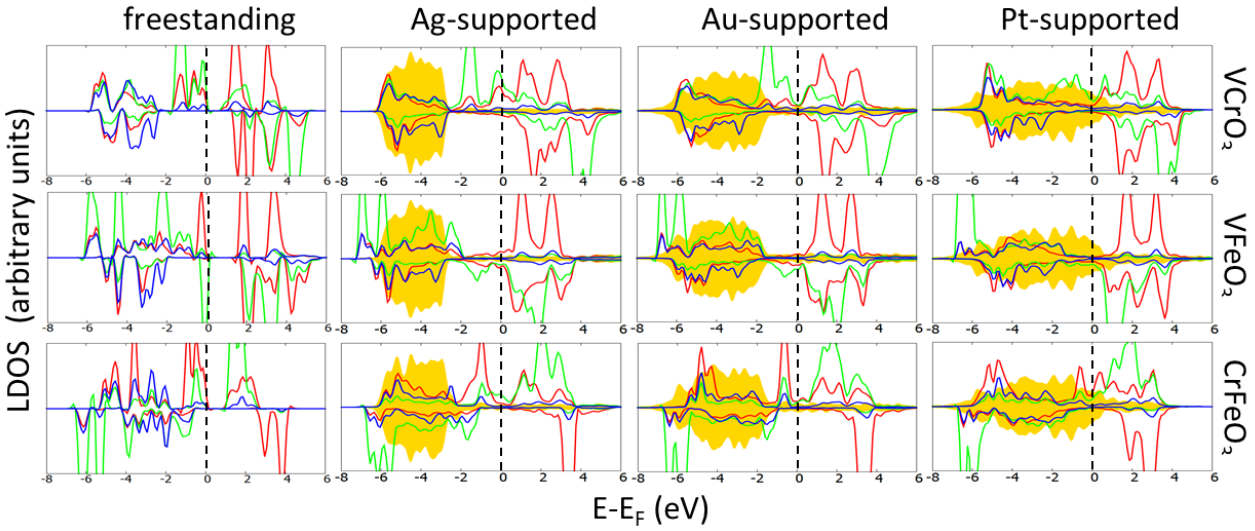

Figure 4: Local densities of states in freestanding and Me-supported mixed MM'O_3 honeycomb monolayers (M = V, Cr; M' = Cr, Fe) projected on M (red), M' (green), O atoms (blue), and substrate atoms (gold shading). A broadening of 0.2 eV has been systematically applied. Vertical dashed lines indicate the position of the Fermi level.

amplitude of R are mainly driven by the behavior of the interface charge transfer Q_{Me}.

Similarly to most supported M_2O_3 parents, the interaction of the mixed films with the metallic substrates gives rise to a systematic electron transfer from the oxide towards the substrate ($Q_{Me} < 0$), but in $CrFeO_3$/Ag where electrons are transferred towards the oxide film ($Q_{Me} > 0$). Both cations and anions contribute to the interface charge transfer and the percentage weight of oxygen contributions progressively increases along the oxide series. At each of the three substrates $|Q_{Me}|$ decreases following the increasing average electronegativity of the two cations ($TiVO_3 < TiCrO_3 < VCrO_3 < TiFeO_3 < VFeO_3 < CrFeO_3$). For each oxide it increases from Ag to Pt in line with the increasing substrate work functions. As a consequence, cation charges $Q_{M,M'}$ increase and oxygen charges $|Q_O|$ decrease when moving from Ag to Pt. Only Q_{Ti} values change particularly little from one substrate to another in all supported TiM'O_3 compounds.

In our previous study on freestanding films,[3] we have pointed out that the electronic modifications in $TiVO_3$, $TiCrO_3$, and $CrFeO_3$ due to mixing are small since their cationic charges and magnetic moments are close to those in the corresponding freestanding parents, and their LDOS differ little from a superposition of the parent LDOS. Conversely, in $TiFeO_3$, $VCrO_3$, and $VFeO_3$, a well pronounced increase of Q_M and a decrease of $Q_{M'}$, correlated with strong modifications of cation magnetic moments and LDOS peak positions with respect to the Fermi level, have been rationalized in terms of mixing-induced redox reactions, leading to $Ti^{4+}Fe^{2+}$, $V^{4+}Cr^{2+}$, and $V^{4+}Fe^{2+}$ oxidation states, respectively.

The presence of the metal substrates visibly alters this picture. In contrast to the freestanding case, supported $TiFeO_3$ displays only negligible mixing-induced electronic modifications, regardless of the metal support (Tab. 2 and 1 and Fig. 2, 3 and 4). Moreover, while, similarly to the freestanding films, the mixing-induced changes in $VFeO_3$ and $VCrO_3$ are the most pronounced, the underlying electron redistributions do not follow the same pattern on the three substrates. Indeed, on Ag and Au substrates, the changes mostly consist of an electron exchange between the two cations ($\delta Q_V \approx -\delta Q_{Cr,Fe}$, Tab. S5), and are associated with opposite shifts of the V and Cr/Fe states in the vicinity of the Fermi level (see Fig. 4). In these mixed oxides also the modifications of oxygen charges δQ_O provide a non-negligible contribution to δQ_{Me}. Conversely, on the Pt substrate the largest modifications concern only vanadium cations, which points toward an increase of the vanadium oxidation state stabilized by an electron transfer towards the metal substrate δQ_{Pt}. These different behaviors illustrate the competition between electron transfer between the two cations and from a cation to the substrate, governed by the availability and nature of the oxide electronic states in the vicinity of the Fermi level. At variance with the above, the electronic characteristics of supported $TiVO_3$ and $TiCrO_3$ films remain relatively close to those of their supported parents, as was the case for their freestanding counterparts. Finally, $CrFeO_3$ displays an intermediate behavior. On Ag and Au, mixing-induced modifications are relatively weak, but on Pt, μ_{Cr} is visibly reduced. These changes, together with the complex DOS modifications (see Fig. 4) do not allow a clear assignment of a change of oxidation state.

To summarize, the structural (R) and electronic (Q_{Me}) characteristics of the supported pure and mixed oxide films follow qualitatively similar trends. The electronic characteristics of $TiVO_3$, $TiCrO_3$, and $TiFeO_3$ correspond closely to a superposition of those of their parents. Conversely, in Ag- and Au- supported $VCrO_3$ and $VFeO_3$ mixing induces an electron transfer from V to either Cr or Fe. It is much stronger in $VFeO_3$ and can be tentatively interpreted as a redox reaction. Interestingly, on the Pt substrate, the electrons are rather transferred from V to the metal substrate. These conclusions are well supported by HSE03 results given in SI, Tab. S8 and Fig. S2.

5 Discussion

In this section, we first discuss the mechanisms which govern the electronic and structural characteristics of metal-supported HC oxides upon interaction with the substrate (Section 5.1) and upon cation mixing (Section 5.2). Then we analyze the evolution of the oxide adhesion (Section 5.3) and mixing (Section 5.4) energies.

5.1 Electron redistribution at the oxide/metal interface

In our recent study on the Au-supported pure M_2O_3 monolayers,[9] we have shown that the interfacial charge transfer Q_{Au} and its consequences on the electronic characteristics of the deposited oxide films may be reliably inferred from the offset between the point of zero charge of the freestanding oxide films E_{ZCP} (approximated by the energy at mid-gap position) with respect to the Fermi level of the bare Au surface $E_F(Au)$ and from the character of the oxide gap edges. We have shown that the decrease of $|Q_{Au}|$ along the series of transition metal oxides is due to the progressive lowering of the point of zero charge, mainly due to the increase of the cation electronegativity. This argument is generalized in Figure 5 to the parents and mixed oxide MLs deposited on the three substrates. Corresponding results from hybrid calculations on Au-supported M_2O_3 and MM'O_3 compounds are reported in SI, Fig. S3.

In agreement with the results of Ref.,[9] we find that, for each substrate and regardless of the pure or mixed oxide character, the interface charge transfer correlates well with $E_F(Me) - E_{ZCP}$. As a consequence, Q_{Me} is systematically the most negative for M_2O_3 oxides with the least electronegative cations (Ti, V), and for mixed oxides with the smallest average cation electronegativity ($TiVO_3$, $TiCrO_3$, and $VCrO_3$). Conversely, small positive Q_{Me} values are found for Cr_2O_3, Fe_2O_3 and $CrFeO_3$. Moreover, for each oxide, the substrate charge becomes more negative along the Ag, Au, and Pt series, following the increase of the work functions of the metal surfaces (4.8 eV, 5.6 eV, and 6.1 eV, respectively). Such quasi-linear behaviour of the interface charge transfer as a function of the band offset agrees well with the predictions of the Metal-Induced Gap States (MIGS) model at metal/semiconductor interfaces.[36,37]

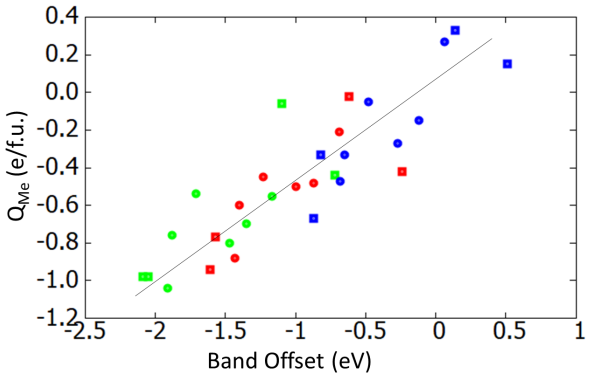

Figure 5: Interface charge transfer Q_{Me} (e/M_2O_3 or MM'O_3 f.u.) as a function of the offset $E_F(Me) - E_{ZCP}$ (eV) between the Fermi level of the bare metal surface and the point of zero charge of the freestanding pure (squares) and mixed (circles) oxide monolayers. Results for Ag, Au, and Pt substrates are plotted with blue, red, and green symbols, respectively. Line is drawn to guide the eye.

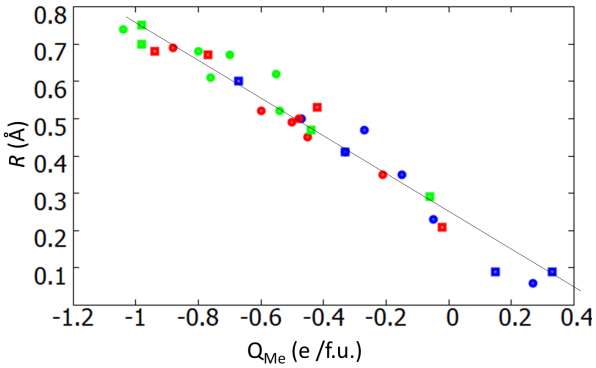

Figure 6: Average rumpling R (Å) in supported pure M_2O_3 (squares) and mixed MM'O_3 (circles) MLs as a function of the electron transfer Q_{Me} (e/M_2O_3 or MM'O_3 f.u.) Results for Me = Ag, Au, and Pt substrates are represented in blue, red, and green, respectively. Line is drawn to guide the eye.

Metal-supported oxide monolayers undergo structural distortions in response to the electrostatic dipole produced by the interface charge

transfer Q_{Me}.[38,39] Based on a simple electrostatic argument, a negatively charged substrate ($Q_{Me} < 0$) repels the anions and thus tends to produce a positive rumpling ($R > 0$) whereas a negative rumpling is expected for a positive charging of the substrate. The induced structural dipole of the oxide film which results from such electrostatic coupling between charge and structure has been baptized induced polarity.[38] In agreement with this argument, we find that, for each substrate and regardless of the pure or mixed oxide character, the film rumpling R correlates very well with the interface charge transfer Q_{Me}. As a consequence, R is systematically the largest for oxides which transfer the largest number of electrons to the metal substrates (Ti_2O_3, V_2O_3, $TiVO_3$). Conversely, the smallest film rumpling is systematically found for Fe_2O_3, Cr_2O_3 and $CrFeO_3$. Moreover, rumpling of each oxide film increases when moving from Ag to Pt, following the corresponding increase of the electron transfer. We stress that such an excellent unique $R \propto Q_{Me}$ relationship obtained for a variety of oxide films on various metal substrates is likely due to a negligible effect of lattice mismatch on R, the latter being rather accommodated by in-plane rotations.

At this point it is worth noting that the monotonic decrease of R is associated with more complex film structure. Indeed, while large rumpling values (large negative Q_{Me}) are systematically associated to an outward relaxation of the three oxygen atoms (per f.u.) with respect to the cation planes, in Fe_2O_3, Cr_2O_3, and $CrFeO_3$ on Ag (the smallest R and positive Q_{Me} values), although R remains positive, two oxygen atoms are located below the average cation positions (SI Tables S1 and S4). In case of oxides which display the smallest negative Q_{Me} (Fe_2O_3 on Au and Pt, $TiFeO_3$/Ag), only one oxygen atom is located below the cation plane or two oxygen atoms are nearly coplanar with the cations.

To summarize, we have shown that the electron transfer between the oxides and the metal substrate is mainly driven by the offset between the oxide band structure (point of zero charge) and the substrate Fermi level. As a consequence, the strongest electron redistributions (large negative Q_{Me}) are found in oxides with the least electronegative cations (Ti and V) deposited on metal substrates with the largest work functions (Au, Pt). Moreover, we find that the interface electron transfer determines the behavior of the substrate-induced film polarization (rumpling) and is responsible for its progressive decrease from the least (Ti_2O_3, V_2O_3, $TiVO_3$) to the most (Fe_2O_3, Cr_2O_3, and $CrFeO_3$) electronegative compounds.

5.2 Electron redistribution upon cationic mixing

While the previous section dealt with the modifications of the oxide ML atomic and electronic structure due to their interaction with the metallic substrates, here we focus on those which take place upon cationic mixing.

In the past we have successfully rationalized the electronic characteristics of mixed bulk MM'O_3 materials,[25] freestanding MM'O_3 honeycomb monolayers,[3] and M_2O_3/M'$_2O_3$ interfaces,[26] from the band offsets between the corresponding parent M_2O_3 and M'$_2O_3$ materials. In the present case, a similar analysis can be based on a comparison between the LDOS of the four metal-supported parents on an energy scale defined by their common vacuum level, Fig. 7. As a reference, the corresponding results for the freestanding HC MLs are recalled. Corresponding HSE03 results on M_2O_3/Au HCs are reported in SI, Figure S4.

The band offset between any couple of parents is quantified by the difference of positions of their Fermi levels $\Delta E_F = E_F(M_2O_3/Me) - E_F(M'_2O_3/Me)$, such that positive and negative values of ΔE_F indicate an initial bias for M_2O_3/Me $\rightarrow$ M'$_2O_3$/Me and M'$_2O_3$/Me $\rightarrow$ M_2O_3/Me electron transfers, respectively. Beyond the relative positions of the Fermi levels ΔE_F, the actual possibility of the charge transfer as well as the precise origin and destination of the transferred electrons also depend on the character of the occupied and empty states in the vicinity of the Fermi level.

While the ordering of Fermi level positions in the freestanding parents was qualitatively determined by the cation electronegativity difference, in the supported ones, it is rather due

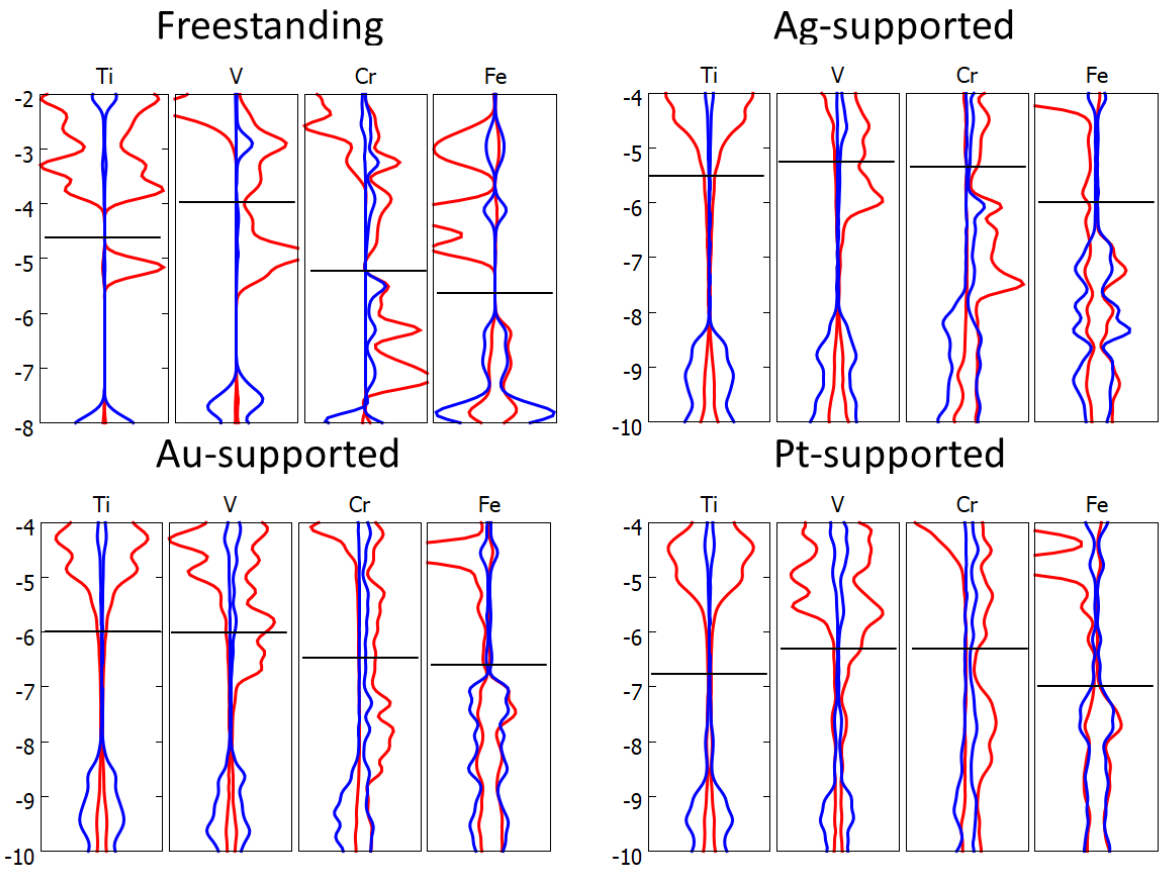

Figure 7: LDOS of the freestanding and Me-supported pure M_2O_3 monolayers (M = Ti, V, Cr, Fe) in the vicinity of their Fermi level (marked by the horizontal black lines), projected on cations (red), and oxygen atoms (blue), on an energy scale obtained by alignment of the common vacuum level. A broadening of 0.2 eV has been systematically applied.

to the change in metal work function induced by the deposition of an oxide film ΔW. Calculated ΔW for the four parents are given in Table 3. We note that, since at each substrate the largest values are systematically found for Fe_2O_3 and the smallest ones for V_2O_3, the resulting ordering of Fermi level positions is not strongly modified compared to that found in the freestanding films.

Table 3: Change of the Metal Work Function ΔW (eV) upon Deposition of Pure HC Monolayers.

	Ti_2O_3	V_2O_3	Cr_2O_3	Fe_2O_3
ΔW_{Ag}	0.62	0.38	0.45	1.15
ΔW_{Au}	0.36	0.44	0.80	0.95
ΔW_{Pt}	0.75	0.15	0.17	0.89

We recall that ΔW is determined by the dipole moment of the oxide/metal interface, which consists of three main contributions.[38,40,41] The first one comes from the reduction of the substrate surface dipole caused by the compression of the spilled-out metal electrons by the deposited oxide monolayer. The second one is induced by the electron exchange Q_{Me} between the oxide film and the metallic substrate. The third one is due to the structural film polarization (rumpling) R. While the first effect produces a negative contribution to ΔW, and while a positive film rumpling ($R > 0$) tends to increase R, the contribution due to electron exchange at the interface either decreases (negative Q_{Me}) or increases (positive Q_{Me}) the substrate work function.

In the present case, the systematically positive signs of ΔW, Tab. 3, suggest that the rumpling contribution is dominant, aided by the charge transfer term in the few cases where Q_{Me} is positive. However, since the largest ΔW values (Fe_2O_3 on the three substrates) systematically correspond to the smallest rumplings R, the behavior of ΔW along the series of oxides is clearly not rumpling-driven. The largest ΔW, responsible for the most pronounced band offsets between parent materials, rather correspond to positive or small negative values of the charge transfer contribution. It should be noted that in-plane rotation ϕ may also play a role since the largest values in Tab. 3 also correspond to the largest rotations.

Solely from the signs of ΔE_F, Fig. 7, one deduces that an electron transfer may systematically occur from Ti_2O_3/Me or V_2O_3/Me toward Fe_2O_3/Me (Me = Ag, Au and Pt) or Cr_2O_3/Au, and from Cr_2O_3/Me toward Fe_2O_3/Me (Me = Ag and Pt). No electron exchange is expected between Ti_2O_3/Me and V_2O_3/Me except on Pt, where an electron transfer from V_2O_3 to Ti_2O_3 could be anticipated. If additionally the character and the density of states at the Fermi level are taken into account, it becomes clear that supported Ti_2O_3 is unlikely to provide electrons to Cr or Fe upon mixing because it has no available occupied cationic d states. Also the electron transfer from V_2O_3 to Ti_2O_3 on Pt is impeded by the absence of empty Ti d states in the energy range between the two Fermi levels. As a consequence, no significant mixing-induced charge redistribution is expected in all Ti-containing compounds. Conversely, since a significant number of occupied cationic states just below the Fermi level exist in V_2O_3/Me, an electron transfer from V_2O_3/Me towards Fe_2O_3/Me is systematically to be expected, as well as a transfer from V_2O_3/Au towards Cr_2O_3/Au. We note that the absence of empty Fe_2O_3 states in the direct vicinity of the Fermi level may produce an electron transfer toward the metal substrate rather than toward the Fe cations. Finally, the limited number of occupied (empty) states at E_F in Cr_2O_3/Me (Fe_2O_3/Me) may hinder electron redistribution in $CrFeO_3$/Me. These predictions correlate very well with the results of the full calculations, Sec. 4.

To summarize, the relative positions of the Fermi levels in the supported parents provide a good guide for understanding the electronic redistributions in the mixed compounds. While the ordering of Fermi levels in the series of parent oxides is not strongly modified by the metal substrate, we have pointed out that the character of the oxide states in the vicinity of the Fermi level is. For the series of supported MM'O_3 HC MLs, the offsets between the parent band structures and the absence of Ti d states in the the Fermi level vicinity

in supported Ti_2O_3 explain why any significant mixing-induced electronic structure modifications are limited to the $VFeO_3$/Me and $VCrO_3$/Me compounds only. The strong increase of vanadium oxidation state suggests an enhanced reactivity of the supported vanadate films, which could thus be of interest in various catalytic reactions, in the same way as the oxygen-rich V_2O_5 oxide is the most important industrial vanadium compound, used as a catalyst.

5.3 Adhesion at the HC/Me interfaces

Table 4 summarizes the adhesion energies E_{adh} (Eq. 1) of pure and mixed oxide monolayers supported on the three metal substrates as well as the misfits between the freestanding layers and metal substrate. Adhesion energies are found to be always positive (favorable to adhesion) and to span a large set of values ranging from about 1.1 eV (Cr_2O_3/Au and $CrFeO_3$/Au) to more than 4.5 eV (Ti_2O_3/Pt and $TiVO_3$/Pt) per formula unit. At each substrate, the adhesion of pure monolayers is systematically stronger for oxides films from the beginning of the series and, for each oxide, it tends to increase from Ag to Pt. E_{adh} of most mixed compounds are smaller than the average values of their parents ($\delta E_{adh} < 0$ in SI, Tab. S6) – the reduction being particularly large for $TiFeO_3$/Me –, but in the case of $TiVO_3$/Pt for which mixing enhances the adhesion ($\delta E_{adh} > 0$).

Since E_{adh} is calculated with respect to the corresponding freestanding oxide films at their equilibrium lattice parameters, it consists of two contributions of different nature. The first one is associated to the elastic strain of the freestanding ML necessary to match its in-plane lattice parameter with the metal substrate (Table 4) and is always unfavorable to adhesion. In the parent series, aside Cr_2O_3 which displays a non-zero rumpling when freestanding and thus a reduced lateral lattice parameter, the misfit decreases from the left to the right of the series (for a given substrate) and from Pt to Ag (for a given oxide) and ranges from about 2% (Cr_2O_3/Ag) to more than 15% (Ti_2O_3/Pt). Misfits of the mixed monolayers show a qualitatively similar behavior and do not exceed the above ranges. However, since the lattice mismatch is accommodated mainly by the in-plane rotations and film rumpling and since the involved distortions require much less energy than bondlength compression, this contribution to E_{adh} displays small variations in each oxide series (of the order of 0.2-0.3 eV/f.u.) and, for a given oxide, its maximum variation between the three substrates is of the order of 0.2 eV/f.u. (SI, Tab. S3). Thus, it is clearly not responsible for the observed large differences of adhesion energies. The second contribution is the energy gained by bringing the strained oxide film in contact with the metal substrate. It directly represents the strength of direct metal-oxide interaction at the interface. It is favorable to adhesion in all considered cases.

While trends in adhesion may not always be easy to rationalize because they involve energy terms of different origin, Figure 8 shows a clear correlation between E_{adh} and the interfacial charge transfer $|Q_{Me}|$. If, in general, a weak/strong charge exchange is indeed often associated with weak/strong interfacial interaction, the present results show the existence of a unique and nearly universal $E_{adh}(|Q_{Me}|)$ curve, which encompasses cases ranging from particularly weakly (Cr_2O_3 and Fe_2O_3 on Ag) to particularly strongly (Ti_2O_3 and V_2O_3 on Pt) interacting interfaces, regardless of the precise nature of the oxide and the metal substrate. This finding clearly demonstrates the dominant role of the direct interfacial interactions in the energetics (second contribution), driven by the cation electronegativity.

5.4 Energetics of mixing

Mixing energies E_{mix} (Eq. 2) have been calculated for the six metal-supported mixed oxide MLs as the energy difference between the mixed systems and the average of the two supported parents. Their values are reported in Table 5, together with the corresponding results for their freestanding counterparts from Ref.[3]

Depending on the oxide, we find negative or

Table 4: Adhesion Energies E_{adh} (eV/f.u.) at the Interfaces Between the Oxide Monolayers and the Three Metal Substrates. Misfits (%) Between the Freestanding MLs and the Underlying Substrates Are Given for Reference.

	Ti_2O_3	V_2O_3	Cr_2O_3	Fe_2O_3	$TiVO_3$	$TiCrO_3$	$TiFeO_3$	$VCrO_3$	$VFeO_3$	$CrFeO_3$
Ag-supported										
E_{adh}	2.52	1.41	1.19	1.64	1.99	1.64	1.61	1.21	1.33	1.32
misfit	10.2	7.9	2.1	7.3	7.3	9.0	8.1	6.4	7.3	6.4
Au-supported										
E_{adh}	3.31	1.91	1.15	1.28	2.62	2.06	1.76	1.60	1.54	1.13
misfit	10.6	8.3	2.4	7.6	7.6	9.4	8.5	6.8	7.6	6.8
Pt-supported										
E_{adh}	4.78	3.75	2.18	2.12	4.50	3.11	2.52	2.92	2.81	1.88
misfit	15.2	12.8	6.7	12.1	12.1	13.9	13.0	11.2	12.1	11.2

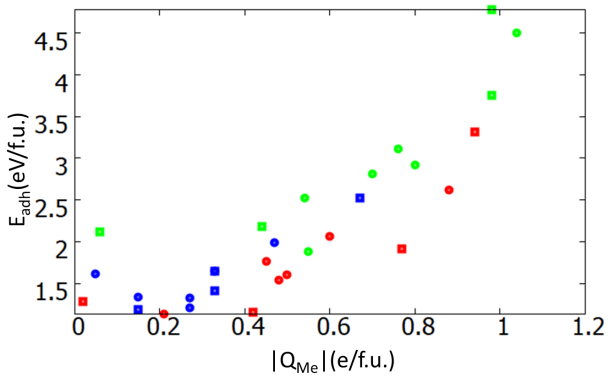

Figure 8: Adhesion energies of pure (squares) and mixed (circles) monolayers on metal substrates E_{adh} (eV/f.u.) as a function of interface charge transfer $|Q_{Me}|$ (e/M_2O_3 or MM'O_3 f.u.). Results for Ag, Au and Pt substrates are represented in blue, red and green, respectively.

positive mixing energies, which represent preference for cationic mixing and phase separation, respectively. If large negative E_{mix} ∼ -0.7 eV/f.u. are found for freestanding $TiFeO_3$ and $VFeO_3$ and for metal-supported $VFeO_3$, in all other cases, the mixing energies are much smaller ($|E_{mix}| < 0.4$ eV/f.u.). We find that, aside few exceptions, for each mixed oxide, the sign of E_{mix} is a relatively robust feature, independent of the substrate, but E_{mix} shows no clear monotonic behavior along the series of oxides or metal substrates.

We recall that in the freestanding case, the large negative mixing energies found for $TiFeO_3$ and $VFeO_3$ have been assigned to the existence of a mixing-induced redox reactions which produce unambiguous changes of cation oxidation states.[3] The same mechanism was also shown to be at work in bulk mixed oxides[25] and at oxide/oxide interfaces.[26] For the metal-supported MLs, this correlation is somewhat less clear, partially due to the difficulty to unambiguously identify the cation oxidation states. However, the large negative E_{mix}, systematically found for $VFeO_3$ on the three substrates, is consistent with the enhanced oxidation of vanadium induced by the electron transfer toward the metal support and/or the Fe cation, as revealed by the features of the interface electronic structure, Sec. 4. Also, the strong reduction of $|E_{mix}|$ in all $TiFeO_3$/Me systems, with respect to their freestanding counterparts, correlates with the suppression of the electron transfer from Ti to Fe when metal-supported. Indeed, the electronic structure results show that the single Ti d electron is systematically transferred to the metal substrate, so that there are no occupied Ti states close to the Fermi level able to transfer electrons to the iron cations.

As to broaden the perspective, Figure 9 gives an overview of the calculated mixing energies in the same series of bulk sesquoxides, freestanding MLs, and metal-supported MLs.[3,25] While a metal substrate enhances the preference for mixing in $VCrO_3$ and reduces it for the Ti-based ones, two systems clearly stand out by their strongly size and support-dependent behaviors. On the one hand, contrary to the bulk phase, the formation of ordered mixed $VFeO_3$ MLs is

Table 5: Mixing Energies E_{mix} (eV/f.u.) of the Six Freestanding[3] and Metal-Supported Mixed HC MLs.

	$TiVO_3$	$TiCrO_3$	$TiFeO_3$	$VCrO_3$	$VFeO_3$	$CrFeO_3$
E_{mix}	+0.32	-0.16	-0.70	-0.14	-0.79	-0.16
E_{mix}(Ag)	+0.12	+0.05	-0.23	-0.22	-0.60	-0.06
E_{mix}(Au)	+0.13	+0.01	-0.17	-0.39	-0.74	-0.08
E_{mix}(Pt)	-0.09	+0.22	+0.23	-0.27	-0.67	+0.12

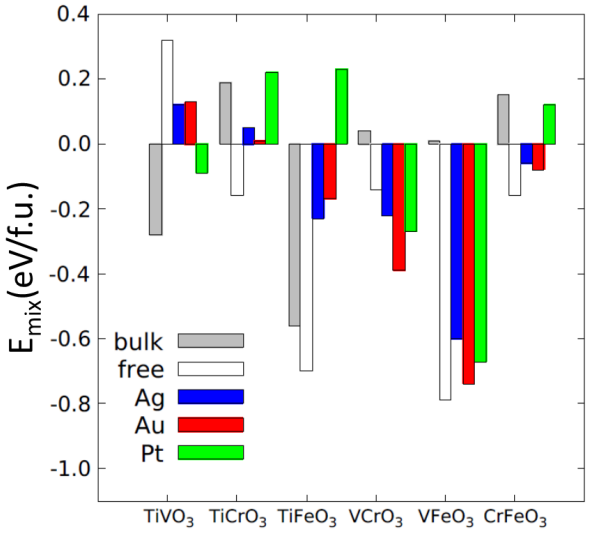

Figure 9: Mixing energies in the series of the six mixed HC oxides. Results for bulk, frestanding, Ag-, Au- and Pt-supported cases are represented in gray, white, blue, red, and green, respectively.

thermodynamically favored not only when freestanding, but also when deposited on a metallic substrate. This opens a promising route for a practical synthesis of this nano-compound. On the other hand, in the perspective of tuning the oxide mixing properties and engineering novel oxide phases, our results show that mixed compounds such as $TiFeO_3$, which are stable in bulk (ilmenite) and freestanding MLs, may be dramatically destabilized by the strong interaction with the metal substrate. Such a strong dependence of mixing behavior on dimensionality and substrate should impact catalytic activity originating from the so-called SMSI (Strong Metal Support Interaction) in which, under reaction conditions, metal particles are encapsulated by an ultra-thin film of the supporting oxide.

6 Conclusion

We have used a DFT+U approach to study how the presence of a metal substrate (Me = Ag, Au, Pt) modifies the structural, electronic and magnetic characteristics of a series of pure M_2O_3 and mixed $MM'O_3$ $3d$ transition metal oxide honeycomb monolayers (M, M' = Ti, V, Cr, Fe).

We have identified general trends in the substrate-induced structural film polarization, film-support electron transfer, and oxide-metal interaction strength, and we have linked them to the behavior of the offsets between the oxide band structure (point of zero charge) and the substrate Fermi level. Accordingly, the strongest interfacial effects are found in pure and mixed oxides with the least electronegative cations (Ti and V) deposited on metal substrates with the largest work functions (Au, Pt). In these cases of Mott-Hubbard oxides, the well pronounced depletion of purely $3d$ Ti and V states has been rationalized by an increase of the cation oxidation state with respect to the 3+ reference.

We have also shown that the relative positions of the Fermi levels in the supported pure oxides provide a good guide for understanding the electronic redistributions in the mixed compounds. However, if the ordering of Fermi levels in the series of parent oxides is only little affected by the metal substrate, the presence of a support significantly modifies the character of oxide states in the vicinity of the Fermi level. As a consequence, aside the general trend for an electron transfer from less (Ti and V) to more (Cr and Fe) electronegative cations, valid in both freestanding and supported monolayers, the metal substrates enhance electron redistributions in V-based compounds and reduce

them in the Ti-based ones. Indeed, the fact that Ti_2O_3 gives all its valence electrons to the metal substrates limits any significant mixing-induced electronic rearrangements to $VCrO_3$/Me and $VFeO_3$/Me only. Depending on the Me substrate, the modifications consist of an electron exchange between the two cations, or between V and the metallic support. Due to the strong modifications of their electronic structure when deposited on metal substrates, these vanadium mixed oxides are expected to display an enhanced reactivity, of possible interest in various catalytic reactions.

These substrate-induced electronic effects have direct consequences on the energetics of cationic mixing. We have shown that, contrary to its bulk phase, the formation of ordered mixed $VFeO_3$ monolayers is thermodynamically favored and that it is not inhibited by the presence of a metal substrate. Conversely, metal support dramatically destabilizes monolayers of $TiFeO_3$, a mixed oxide which is stable in bulk (ilmenite). Thus, not only our results show that metal substrates can indeed be used for engineering novel oxide phases by cationic mixing, but they also provide well-founded general guidelines on the link between support characteristics, the oxide electronic structure, and the preference for mixing or phase separation in the supported oxide films.

7 Acknowledgment

We acknowledge fruitful discussions with M. R. Castell, S. Wang and N. Nilius.

8 Supporting Information Available

The Supporting Information contains:

- full DFT+U results for parent M_2O_3/Me MLs (Tabs. S1-S3) and for mixed MM'O_3/Me MLs (Tabs. S4-S6);
- HSE03 results for parent M_2O_3/Au MLs (Tab. S7, Fig. S1) and for mixed MM'O_3/Au MLs (Tab. S8, Fig. S2). Figs. S3-S4 are the HSE03 equivalents of Figs. 5 and 7 in the main text;

This material is available free of charge via the Internet at http://pubs.acs.org.

References

(1) Freund, H.-J.; Pacchioni, G. Oxide ultrathin films on metals: new materials for the design of supported metal catalysts. *Chem. Soc. Rev.* **2009**, *37*, 2224–2242.

(2) Netzer, F. P.; Fortunelli, A.; Eds., *Oxide materials at the two-dimensional limit*; Springer Series in Materials Science; Springer International Publishing: Cham, Switzerland, 2016; Vol. 234.

(3) Goniakowski, J.; Noguera, C. Intrinsic properties of pure and mixed monolayer oxides in the honeycomb structure: M_2O_3 and MM'O_3 (M, M' = Ti, V, Cr, Fe). *J. Phys. Chem. C* **2019**, *123*, 7898–7910.

(4) Surnev, S.; Sock, M.; Kresse, G.; Andersen, J. N.; Ramsey, M.; Netzer, F. Unusual CO adsorption sites on vanadium oxide-Pd(111) "inverse model catalyst" surfaces. *The Journal of Physical Chemistry B* **2003**, *107*, 4777–4785.

(5) Plessow, P. N.; Bajdich, M.; Greene, J.; Vojvodic, A.; Abild-Pedersen, F. Trends in the thermodynamic stability of ultrathin supported oxide films. *The Journal of Physical Chemistry C* **2016**, *120*, 10351–10360.

(6) Barcaro, G.; Agnoli, S.; Sedona, F.; Rizzi, G. A.; Fortunelli, A.; Granozzi, G. Structure of reduced ultrathin TiO_x polar films on Pt(111). *J. Phys. Chem. C* **2009**, *113*, 5721–5729.

(7) Pomp, S.; Kuhness, D.; Barcaro, G.; Sementa, L.; Mankad, V.; Fortunelli, A.; Sterrer, M.; Netzer, F. P.; Surnev, S. Two-dimensional iron tungstate: A ternary oxide layer with honeycomb geometry. *J. Phys. Chem. C* **2016**, *120*, 7629–7638.

(8) Tumino, F.; Carrozzo, P.; Mascaretti, L.; Casari, C. S.; Passoni, M.; Tosoni, S.; Bottani, C. E.; Bassi, A. L. Two-dimensional TiOx nanostructures on Au (111): a scanning tunneling microscopy and spectroscopy investigation. *2D Materials* **2015**, *2*, 045011.

(9) Goniakowski, J.; Noguera, C. Properties of M_2O_3/Au(111) honeycomb monolayers (M = Sc, Ti, V, Cr, Mn, Fe, Co, Ni). *J. Phys. Chem. C* **2019**, *123*, 9272–9281.

(10) Wu, C.; Marshall, M. S. J.; Castell, M. R. Surface structures of ultrathin TiO_x films on Au(111). *J. Phys. Chem. C* **2011**, *115*, 8643–8652.

(11) Wang, S.; Hu, X.; Goniakowski, J.; Noguera, C.; Castell, M. R. Influence of the support on stabilizing local defects in strained monolayer oxide films. *Nanoscale* **2019**, *11*, 2412–2422.

(12) Wang, S.; Goniakowski, J.; Noguera, C.; Castell, M. R. Atomic and electronic structure of an epitaxial Nb2O3 honeycomb monolayer on Au (111). *Physical Review B* **2019**, *100*, 125408.

(13) Köksal, O.; Baidya, S.; Pentcheva, R. Confinement-driven electronic and topological phases in corundum-derived 3*d*-oxide honeycomb lattices. *Phys. Rev. B* **2018**, *97*, 035126.

(14) Möller, C.; Fedderwitz, H.; Noguera, C.; Goniakowski, J.; Nilius, N. Temperature-dependent phase evolution of copper-oxide thin-films on Au(111). *Phys. Chem. Chem. Phys.* **2018**, *20*, 5636–5643.

(15) Wu, C.; Castell, M. R.; Goniakowski, J.; Noguera, C. Stoichiometry engineering of ternary oxide ultrathin films: $Ba_xTi_2O_3$ on Au(111). *Phys. Rev. B* **2015**, *91*, 155424.

(16) Kresse, G.; Furthmuller, J. Efficient iterative schemes for ab initio total energy calculations using a plane-wave basis set. *Phys. Rev. B* **1996**, *54*, 11169–11186.

(17) Kresse, G.; Hafner, J. Ab initio molecular dynamics for liquid metals. *Phys. Rev. B* **1993**, *47*, 558–561.

(18) Blöchl, P. E. Projector augmented-wave method. *Phys. Rev. B* **1994**, *50*, 17953–17979.

(19) Kresse, G.; Joubert, D. From ultrasoft pseudopotentials to the projector augmented-wave method. *Phys. Rev. B* **1999**, *59*, 1758–1775.

(20) Dion, M.; Rydberg, H.; Schroder, E.; Langreth, D. C.; Lundqvist, B. I. Van der Waals density functional for general geometries. *Phys. Rev. Lett.* **2004**, *92*, 246401.

(21) Klimes, J.; Bowler, D. R.; Michaelides, A. Chemical accuracy for the van der Waals density functional. *J. Phys.: Cond. Matt.* **2010**, *22*, 022201.

(22) Klimes, J.; Bowler, D. R.; Michaelides, A. Van der Waals density functionals applied to solids. *Phys. Rev. B* **2011**, *83*, 195131.

(23) Anisimov, V. I.; Aryasetiawan, F.; Liechtenstein, A. I. First-principles calculations of the electronic structure and spectra of strongly correlated systems: the LDA+U method. *J. Phys.: Condens. Matter* **1997**, *9*, 767–808.

(24) Dudarev, S. L.; Botton, G. A.; Savrasov, S. Y.; Humphreys, C. J.; Sutton, A. P. Electron-energy-loss spectra and the structural stability of nickel oxide: An LSDA+U study. *Phys. Rev. B* **1998**, *57*, 1505–1509.

(25) Le, H.-L. T.; Goniakowski, J.; Noguera, C. Properties of mixed transition metal oxides: MM'O_3 in corundum-type structures (M, M' = Al, Ti, V, Cr, and Fe). *Phys. Rev. Mat.* **2018**, *2*, 085001.

(26) Le, H.-L.; Goniakowski, J.; Noguera, C. (0001) Interfaces between M_2O_3 corundum oxides (M = Al, Ti, V, Cr, Fe). *Surf. Sci.* **2019**, *679*, 17–23.

(27) Heyd, J.; Scuseria, G.; Ernzerhof, M. Hybrid functionals based on a screened Coulomb potential. *J. Chem. Phys* **2003**, *118*, 8207–8215.

(28) Heyd, J.; Scuseria, G.; Ernzerhof, M. Erratum: "Hybrid functionals based on a screened Coulomb potential" [J. Chem. Phys. 118, 8207 (2003)]. *J. Chem. Phys* **2006**, *124*, 219906–219906.

(29) Prada, S.; Giordano, L.; Pacchioni, G.; Noguera, C.; Goniakowski, J. Properties of Pt-supported iron oxide ultra-thin films: Similarity of Hubbard-corrected and hybrid density functional theory description. *J. Chem. Phys.* **2014**, *141*, 144702.

(30) Nilius, N.; Fedderwitz, H.; Gross, B.; Noguera, C.; Goniakowski, J. Incorrect DFT-GGA predictions of the stability of non-stoichiometric/polar dielectric surfaces: the case of $Cu_2O(111)$. *Phys. Chem. Chem. Phys.* **2016**, *18*, 6729–6733.

(31) Prada, S.; Giordano, L.; Pacchioni, G.; Goniakowski, J. Theoretical description of metal/oxide interfacial properties: The case of MgO/Ag(001). *Appl. Surf. Sci.* **2016**, *390*, 578–582.

(32) Bader, R. F. W. A quantum theory of molecular structure and its applications. *Chem. Rev.* **1991**, *91*, 893–928.

(33) Henkelman, G.; Arnaldsson, A.; Jonsson, H. A fast and robust algorithm for Bader decomposition of charge density. *Comput. Mater. Sci.* **2006**, *36*, 354–360.

(34) Momma, K.; Izumi, F. VESTA 3 for three-dimensional visualization of crystal, volumetric and morphology data. *J. Appl. Crystallogr.* **2011**, *41*, 1272–1276.

(35) Monkhorst, H.; Pack, J. Special points for Brillouin-zone integrations. *Phys. Rev. B* **1976**, *13*, 5188–5192.

(36) Flores, F.; Tejedor, C. On the formation of semiconductor interfaces. *Journal of Physics C: Solid State Physics* **1987**, *20*, 145–175.

(37) Bordier, G.; Noguera, C. Electronic structure of a metal-insulator interface: Towards a theory of nonreactive adhesion. *Phys. Rev. B* **1991**, *44*, 6361–6371.

(38) Goniakowski, J.; Noguera, C. Polarization and rumpling in oxide monolayers deposited on metallic substrates. *Phys. Rev. B* **2009**, *79*, 155433.

(39) Goniakowski, J.; Noguera, C.; Giordano, L.; Pacchioni, G. Adsorption of metal adatoms on FeO(111) and MgO(111) monolayers: Effects of charge state of adsorbate on rumpling of supported oxide film. *Phys. Rev. B* **2009**, *80*, 125403.

(40) Giordano, L.; Cinquini, F.; Pacchioni, G. Tuning the surface metal work function by deposition of ultrathin oxide films: Density functional calculations. *Phys. Rev. B* **2006**, *73*, 045414.

(41) Giordano, L.; Pacchioni, G.; Goniakowski, J.; Nilius, N.; Rienks, E. D. L.; Freund, H.-J. Interplay between structural, magnetic, and electronic properties in a FeO/Pt(111) ultrathin film. *Phys. Rev. B* **2007**, *76*, 075416.

Graphical TOC Entry